DEVELOPMENT OF A MULTI-BLOCK/OVERSET GRID SOLVER

Hamid Reza KHEIRANDISH* and Jiro NAKAMICHI**
***Research Center of Computational Mechanics, Inc., Tokyo, Japan,**
****Japan Aerospace Exploration Agency**

Keywords: *SST, Unsteady Flow, Multi-Block, Overset Grid*

Abstract

A new code for aeroelasticity simulations based on Multi-Block and Overset grid concept was developed. This code, like the original single-block solver, is based on the Navier-Stokes equations coupled with a turbulence model and structural equations. Its applicability and reliability were verified in different test cases through comparative computations with results of other methods. This code will be applicable to complicated configuration and can operate on parallel machine. In this paper, comparative computations in JAXA and DLR with experiment around a SST type wing in unsteady flow, to investigate the control surface behavior in transonic region, are presented in the first. Secondly the new code verifications for multi-block/overset grid configurations are presented.

1 Introduction

The predictions of detailed steady/unsteady flow field around full configuration of aircraft and the associated aerodynamic forces and moments are always challenging task to designers. Through the rapid development of capability of computational fluid dynamics (CFD) and computer hardware technology, comprehensive flow field computation around the complicated configurations has been considered feasible. Recently, the accuracy of computed results has been improved significantly. In addition, computational efficiency has been substantially enhanced through rapid development of effective geometry modeling/grid generation methods and advanced numerical algorithms of CFD technology. However, it is important for a designer/researcher that an effective analytical tool is available to evaluate the flow field and the forces acting on the considered configuration. As an example, adding engines/nacelles to a clean wing make the computational works substantially increase. Two factors responsible for this are difficulty of surface geometry modeling at the intersection between wing and engines/nacelles and cumbersome of generation of a smooth, continuous, structured computational grid. These problems typically lead to considerably more work and time. This paper describes an effort to develop a new solver based on overset and multi-block grid concept, to overcome these obstacles.

The Chimera scheme allows for a system of relatively simple grids, each conforming to a single component of a complex surface, to be combined into a composite grid. A complex surface is surrounded by a collection of grids, each of which resolves some segment of the flow, while the composite of all the grids covers the entire domain. The grids overlap each other in an unstructured fashion. Flow information is transmitted from one grid to another by means of the common, overlapping volume.

Multi-block method is an approach in which can break a complicated geometry into sub-domains (blocks) with simple shapes. Structured grids then can be generated within each block independently. The solution domain is decoupled into several blocks accordingly. Governing equations can be solved in each sub-domain independently. In order to link the solutions in every block and recover the coupling, iterations between the blocks are needed. There are certain advantages of using multi-block or overset grid methods; (1) By breaking physical domain into blocks the geometric topology complexity can be greatly reduced. (2) We will have more freedom in local grid. More grids can be put in high gradient region without wasting computational resource in other zones. (3) With structural grids used in each block, standard structured flow solvers can be used. (4) This approach provides a natural routine for parallel computing.

We have recently developed a multi-block/overset aeroelastic solver for computing problems that cannot fit in a single-block grid. At this phase our multi-block solver uses the patched-grid concept. In this concept grids at each block boundary meet each other along a common line(surface) and do not overlapped. The overlapped-grid uses the Chimera method concept. The Chimera procedure is divided into two parts: (1) the generation of the composite grid and associated connection and interpolation of data and (2) the solution of the flow model appropriate to each mesh. In our procedure, at this stage, to facilitate data transformation in parallel computation, an overlapped grid must be inside of just one block.

For multi-block solver user must provide the grid-blocks, intersection information, type of boundaries, body surface grouping and PE-Blocks distributions. For overlapped grid solver user must provide the hierarchy, non-penetrating surfaces and normal vectors to the body surfaces. In this paper we explain firstly the validation effort of the single-block solver and then about the new solver.

2 Details of Scheme

The core of CFD code for aeroelasticity simulation is a single-block structured grid solver based on the 3D thin-layer approximated Navier-Stokes equations with the Baldwin-Lomax turbulence model[1] for the flow field and a modal approach formulation for the structural dynamics. The integration is performed employing the second-order accurate upwind TVD scheme[2] for the flow field equations and the Wilson's θ method for the equations of motions of the structure. The integration of the flow equations for unsteady cases is preceded on dynamic grids, in a time accurate manner. The grids are regenerated at each time step fitting the instantaneous position and the deformation of the wing. More details will be found in reference [3].

The improved version of this code can treat multi-block and overlapped grid in the following manner. The Chimera grid concept[4] is used for treatment of overlapped grids. In order to implement a Chimera method, it is necessary to impose structure on the aggregate of grids. The hierarchical form used here, to facilitate the data communication between grids in parallel computation formed by MPI, is to limit each grid lied totally inside precursor grid. There are two major steps in the Chimera scheme to establish inter-grid communication: (1) Hole-cutting, which essentially involves blanking cells of a grid in regions that overlap with Non-Penetrating-Surfaces (NPS) of the other grids and identifying Chimera boundary cells that lie along the hole (Fringe-Boundary-Surfaces FBS) as well as Interpolation Boundary Surfaces IBS. (2) Identifying interpolation stencils, which involve finding donor cells for the Chimera boundary cells in each grid and interpolating the solution from donor cells to the boundary cells.

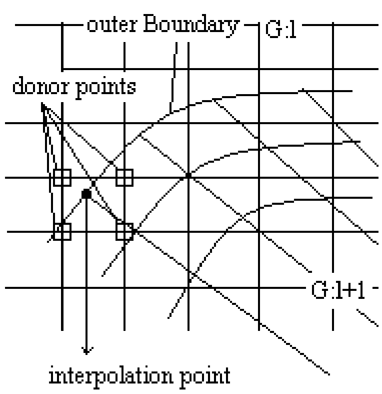

Fig. 1. Interpolation at outer Boundary

The donor points (grid nodes) are selected as the vertices of the cell where interpolation point lays inside (in 3D, 8 points). Figures 1 and 2 show the Chimera concepts. Implementation of overlapped grid needs to define (1) NPS, usually the solid

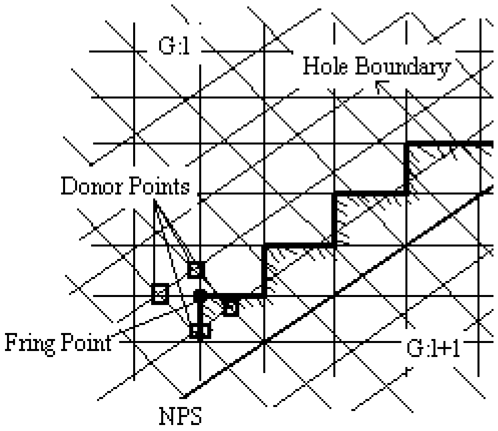

Fig. 2 Interpolation at Hole Boundary

wall boundaries in each grid, (2) interpolation boundary surfaces (IBS), usually the outer boundary of child grid and (3) the hierarchy of grids. The computation proceeds for each grid individually where the points marked as hole are nullified. The transformation of information will be done through the interpolation between interpolation points and their donor grid points.
A patched grid multi-block concept is used here. In this concept the grids at each block boundary meet each other along a common line(surface) and do not overlap. The outer boundaries of each block are considered as a window. Each window can contain both physical boundary and inter-block boundaries. The data communications take places through the inter-block boundaries. For multi-block solver user must provide grid-blocks, intersection information, type of boundaries, body surface grouping and PE-blocks distributions data.

3 Validation and Evaluation of CFD Codes

The single-block solver has been already used in many research topics. Some of them are presented previously in [3,7]. In the most recent effort, an inter-code verification has been done between JAXA (Japan Aerospace Exploration Agency) and DLR (German Aerospace Center). In this effort the computational results are compared with the wind tunnel experimental data. In the first some of the results of this cooperative work is presented. The next is verification of new multi-block/overset code applied for various types of configuration.

3.1 Inter-code verification

One of the research topics still open to treat in the CFD area is to develop precise analytical code to calculate unsteady aerodynamics in transonic region due to control surfaces oscillation. The estimation of the aerodynamics of the control surfaces is difficult because the control surfaces are usually equipped along trailing edge and often are embedded in a developed boundary layer. This research aims validation and/or improvement of the CFD codes through comparisons between codes and experimental data and an investigation on the behavior of control surface on the SST (Supersonic Transport) type wing configuration.

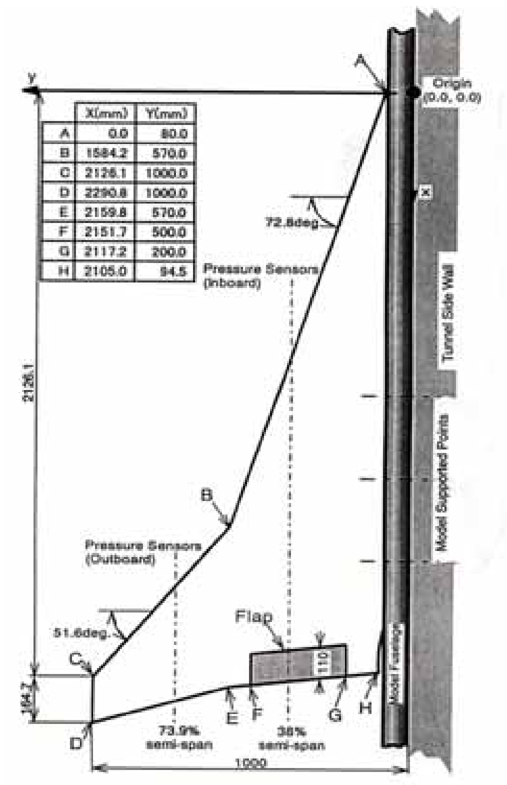

Fig. 3. Plan-view of SSTW Model

3.1.1 Outline of Test Model

The model is an elastic semi-span SST-type wing (SSTW) attached to a rigid fuselage model.

The leading edge is double-swept-backed as shown in figure 3. This wing has the NACA0003 airfoil section at each semi-span station. The unsteady flow fields are generated by harmonic oscillation of the aileron driven by an electric motor. The lowest natural frequency of the model is about 10 Hz in rest air. The total number of the pressure orifices is 46. The dynamic deformation of the model and the unsteady aerodynamics were measured in the tests. The experimental results have already been published in [5]. The six tested cases, at Mach number 0.9 and 0.98 with the aileron frequencies from 5 to 25 Hz, have been selected as the validation data. One of them is presented here. The tests were done at JAXA 2m x 2m Transonic Wind Tunnel. The plan form and the dimensions of the model are shown in figure 3.

Table 1. Summarized of Computed Cases

Case	M	δ_0	δ_{amp}	F	R/E		Exp
s-1	0.9	0	—	—	R	N/D	O
s-2	0.9	5	—	—	R	N/D	O
s-3	0.98	0	—	—	R	N/D	—
u-1	0.9	0	2	5	R	N/D	O
u-2	0.9	0	2	15	R	N/D	O
u-3	0.9	0	2	25	R	N/D	O
u-4	0.9	5	2	25	R	N/D	O
u-5	0.98	0	2	15	R	N/D	—
u-6	0.9	0	2	15	E	N	O

s : Steady , u : Unsteady , M : Mach Number, F : Frequency(Hz)

δ_0 Aileron Mean deflection, δ_{amp} Amplitude of the Aileron

R/E : Rigid or Elastic Wing Computation

3.1.2 CFD Methods

The present CFD code is the single-block solver explained previously. The CFD code employed by DLR is based on the 3D Euler equations with integral boundary layer coupling. The Euler solver uses an upwind scheme based on Wegner's Riemann solver[6]. The time integration is performed on dynamic grids applying the virtual grid deformation technique. The boundary layer equations are solved in streamline direction at every time step. The obtained boundary layer thickness is taken into account to correct the solid-wall boundary condition. In the virtual grid deformation technique the actual grid points are not needed. The gradients of the metrics of the grid system and the grid speeds at each time step are used during the unsteady computations. These quantities are interpolated in space and can be obtained by sufficiently small additional computing time.

3.1.3 Comparison of Results

The computed cases are summarized in Table 1. The Reynolds number is fixed to 12 millions in all the computed cases. The computed steady pressure distributions at Mach number 0.9 are shown in figures 4 and 5 in comparisons with the experimental results. The angle of attack of the main surface is 0^o in all cases. The figures 4-5 show the cases with the mean deflection angles of the aileron (DAoA) 0^o and 5^o . In most of the tested cases, there existed no supersonic regions on the main or aileron surface and accordingly no shock waves were established. It is well known that the shock waves on the wing surface have a significant role in the transonic unsteady aerodynamics and they cause the non-linearity. An H-H mesh topology with 0.8 million grid points was used in the present computations. The DLR computations were performed on a C-H mesh with .3 million grid. There are some discrepancies between the computational results and the experimental ones near the hinge line of the control surface. The computed wing section geometry is not completely compatible with the actual model at the upstream gap (which is not simulated in the numerical grid model) of the aileron. At 75% semi-span station(the section without aileron), the agreement is much better .

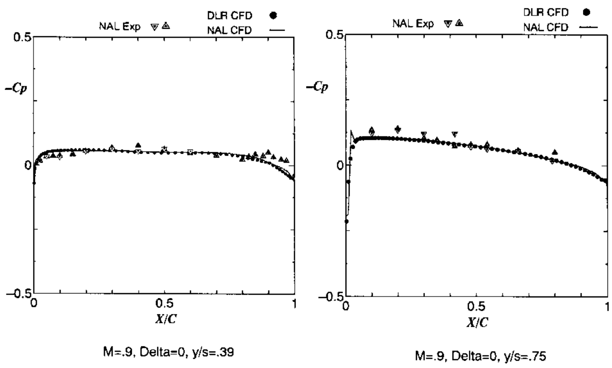

Fig. 4. Steady Pressure Distributions

SSTW, M=.9, α=0.0, δ=0.0, R_e=1.2$\times 10^7$

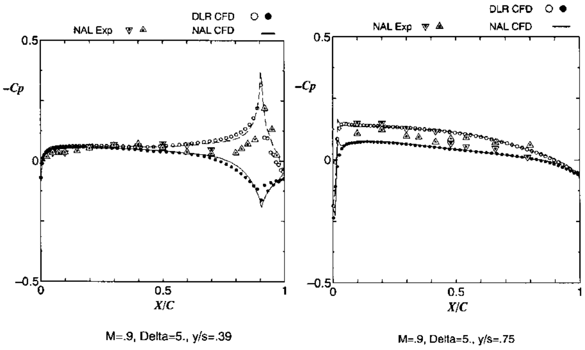

Fig. 5. Steady Pressure Distributions
SSTW, M=.9, α=0.0, δ=5.0, R_e=1.2$\times 10^7$

In figure 5, the result at the DAoA 5^o is shown. The measured pressure distributions do not coincide with the computed results concerning the pressure peak position, while the computed results agreed with each other. This is considered due to the same reason as mentioned in the above. At 75% semi-span station, the experimental results are scattering, but they are relatively in good agreements with the CFD results.

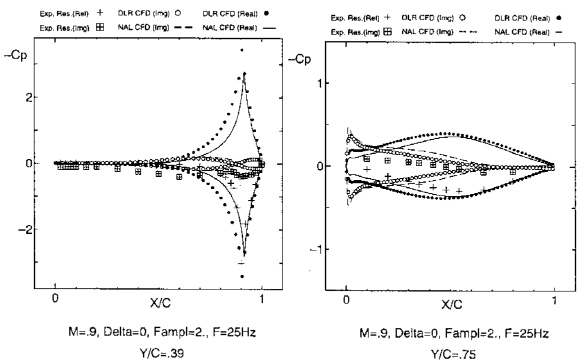

Fig. 6. Unsteady Pressure Distributions, M=.9, α =0.0, δ =0.0, R_e=1.2$\times 10^7$, F=25Hz, δ_{amp}=2.

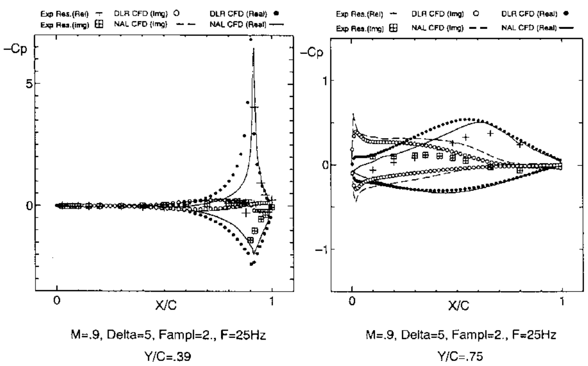

Fig. 7. Unsteady Pressure Distributions, M=.9, α =0.0, δ =5.0, R_e=1.2$\times 10^7$, F=25Hz, δ_{amp}=2

The unsteady pressure distributions are decomposed into real and imaginary parts with respect to the aileron motion. For the unsteady cases, the experimental data are given only for the upper surface. The amplitude of the oscillation of the aileron is 2^o around the DAoA in all cases. In figure 6, the results of case No.U3 are shown.

There are differences between the results obtained by CFD codes just upstream region of the hinge line. The similar trend exists in the other cases, too. The real parts computed by present code are in a better agreement with the experimental data. One of the reasons might be; the difference in governing equations in each codes; the other possible reason might be the difference in hinge line position in each computational grids. The estimated boundary-layer thickness for the correction by DLR might be larger than that computed by the present code solving the NS equations. At 75% semi-span station, the experimental results are far apart from the computed results. It comes from the fact that the pressure distributions were measured on the elastic wing while the wing is assumed rigid in the numerical simulations. Figure 7 shows the case No.U4, in which the DAoA was taken to be 5^o. In the cases of U1-U3, no significant supersonic regions were seen on the surface, though it was expected a supersonic region appears especially on the aileron surface. It can be confirmed from the steady pressure distributions (figure 4) that the Cp is larger than the Cp critical,-.1879 at M=0.9 , on the aileron surface.

3.2 Multi-block/overset grid solver verification

In this section, explanations about the verification results obtained by the new code are presented. Generating high quality single-block structured grid for complicated configurations like aircraft with engines/pylons/nacelles, external stores and, rotary wing and etc, is too hard or sometimes impossible. To overcome difficulties that arise in grid generation for the complicated configuration, the multi-block or overset grid techniques is recommended for the

structured grid. Though for a CFD solver, dealing with one-block grid is straightforward and usually presents the best obtainable performances.
Regarding the amount of memory and runtime requirements for a large-scale problem, parallelization of CFD code is inevitable. Fortunately parallelization of a multi-blocks solver can be done in an easer trend. This new code can work on parallel machines using MPI.
Here the test cases results and comparisons are presented. All the computations at this stage are based on the Euler equations.

3.2.1 Two Dimensional Overset Grid test

In the first, a single-block two-dimensional grid around an airfoil and its correspondence in overset grid topology is considered. The airfoil section selected here is NACA0012. The single-block grid uses an O-type grid with 161×40×3 mesh points and outer boundary is put 20 times chord-length far away from the airfoil surface. The overset grid consists of an O-type grid(101 × 31 × 3) inserted on a Cartesian type background grid(51 × 51 × 3). The outer boundary of O grid in the overset system is set at just about 3 times of chord- length. The background grids are more clustered near the airfoil. The pressure distributions at Mach number 0.8 and angle of attack (AoA) 1.25^o, are compared with each other and with the results obtained by other solvers[8,9]. The results are shown in figure 8. The agreements between the present two different computations and the references are extremely good.

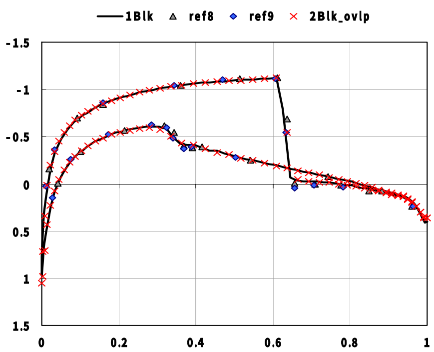

Fig. 8. Pressure Distributions around NACA0012, *M*=.8, α =1.25

The shock strength and position on the upper and lower surfaces coincide with each other well. Figure 9, shows the case in which unsteady flow computation is verified. The airfoil is forced to oscillate in pitch around the quarter chord. In this computation, the background grid is fixed while the grid around the airfoil (O grid) is updated at each time step. The Holes, IBS, FBS and Donor grids are updated at each time step, too. The pitch motion amplitude around the mean angle of attack and the reduced frequency are .25^o and 0.25. The reduced frequency is based on free-stream flow velocity and half-chord-length. This case shows the accuracy of overset grid strategy in unsteady flow computations. The unsteady pressures, computed by two different grid topologies, are decomposed into real and imaginary parts and are compared with each other. The comparisons show good agreements between the methods.

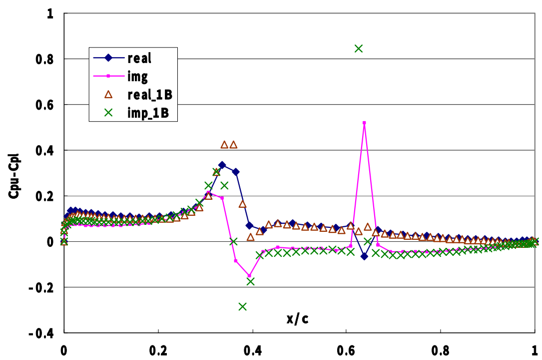

Fig. 9. Comparison of Unsteady Pressure Distributions Between Single Grid and Overset Grid NACA0012, *M*=.8, α =1.25, R_f=.25, α $_{amp}$=.25

3.2.2 Three Dimensional Overset Grid Test

This example shows the future possibility of computation with this type of overlapped grid. A pylon-wing (YXX wing) configuration is considered and steady state result was computed. The grid view and pressure distributions are given in figures 10. The pylon is inserted in YXX grid just under the section of the wing-kink position. The length of the engine/nacelle is about 1.5 times of the local chord-length of the wing. The computed pressure distributions for engine-pylon-nacelle are shown at top and bottom of it in stream-wise direction in figure

11. The pressure distributions for YXX wing are presented at two span-wise positions. One is selected as just right upper of the pylon and another one far away from it. There can be seen a strong shock wave on the lower surface of this wing near the pylon, while there are no shock waves on the lower surface of the clean YXX at the same flow conditions.

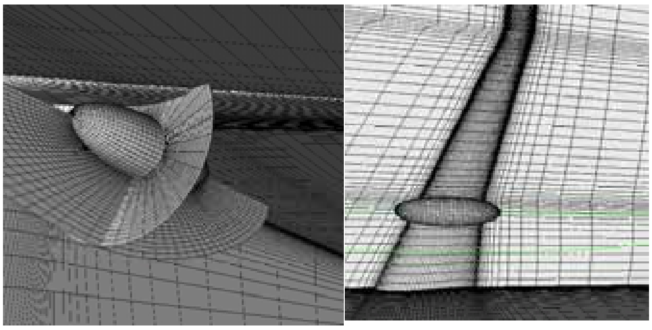

Fig. 10. Schematic view of Wing-Pylon overset Grid

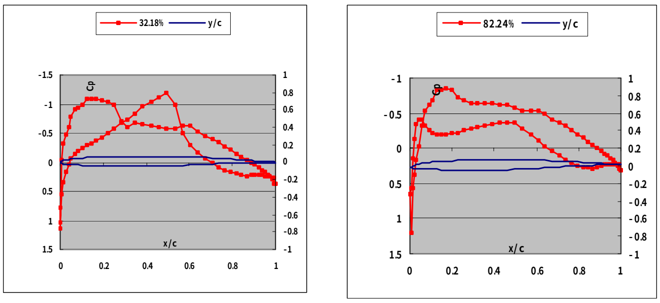

Fig. 11. Pressure Distributions For Wing-pylon Configuration M=.7, α =-.82

3.2.3 Multi-Block Test Cases

A wing-engine wind tunnel test model was selected for capability verification of the multi-block solver. This model was designed for investigation and estimation of flutter of the engine powered experimental SST (SuperSonic Transport) developed at the JAXA. To prevent the effects of the wind tunnel wall boundary layer and to facilitate mounting system of the model, a cylindrical fuselage with blunt nose was manufactured. A structured multi-blocks mesh with 240 blocks and 1.3 millions grid points for half-span model was generated. Surface grids on this model are shown in figure 12. The blocks distributions on the surface can be distinguished by variation of the colors. At this stage, the steady state solutions were computed. The flutter simulation will be done in near future. Steady state flow results at three different Mach number, 0.7,0.8 and 0.9 at zero angle of attack are illustrated here. The outer boundaries are set far away enough to prevent shock reflection from outer boundaries. The computations were done on a PC with PIV 800MHz CPU. It takes a couple of hours to get steady flow results. There is no flow through the engine in this test model.

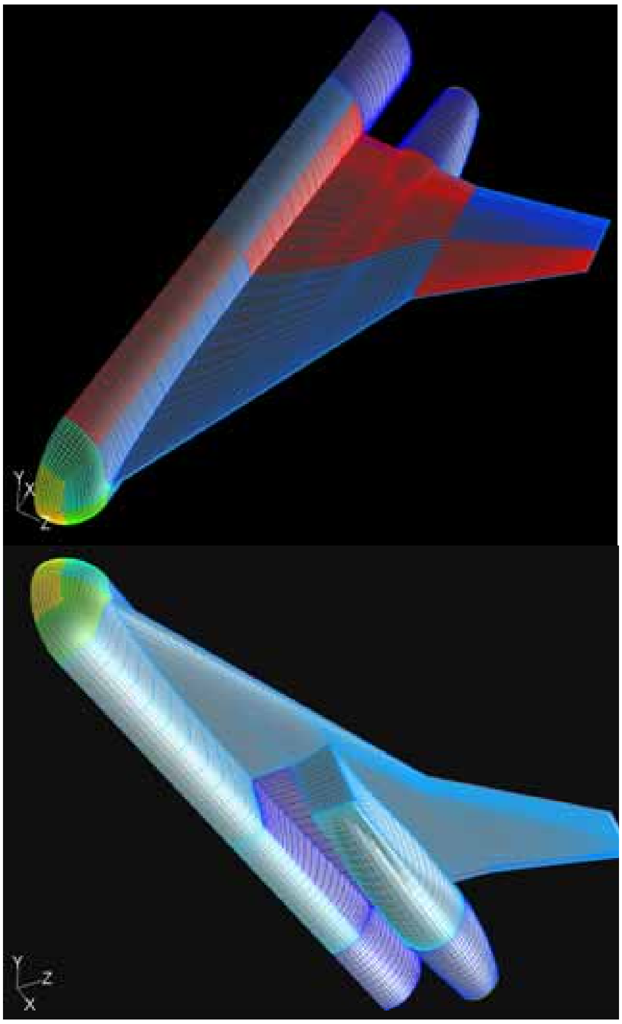

Fig. 12. Schematic View of the test model and generated surface grids(upper and lower view)

The steady flow Pressure distributions are given at different semi-span stations, which are illustrated in the figure 13. The first span-section stands on body surface (8% semi-span), the third one on the wing-engine surfaces (38% semi-span). The pressure coefficient distributions on surfaces and at the span sections are given in figures. 14-22. Figures 14,15 show the pressure coefficient contours on upper and lower surfaces at Mach number 0.7. The Cp critical at Mach number 0.7 is –0.7791. Pressure coefficient distributions at various semi-span positions are given in figure 16. It is noted that the supersonic regions appeared only near the body nose in a very small area. A weak shock wave appeared at this area. Pressure contours and distributions at Mach number 0.8 are given in figures 17 and 18. The critical pressure coefficient is –0.435. Supersonic regions appeared near the body nose and engine

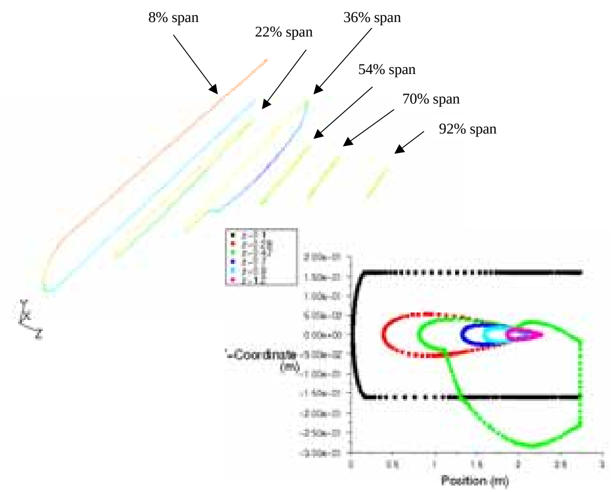

Fig. 13. Semi-Span Stations Illustration

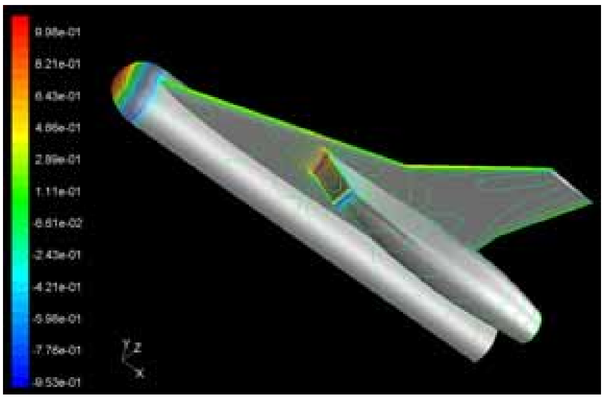

Fig. 14. Pressure Coefficient Contours M=.7, α =0.0

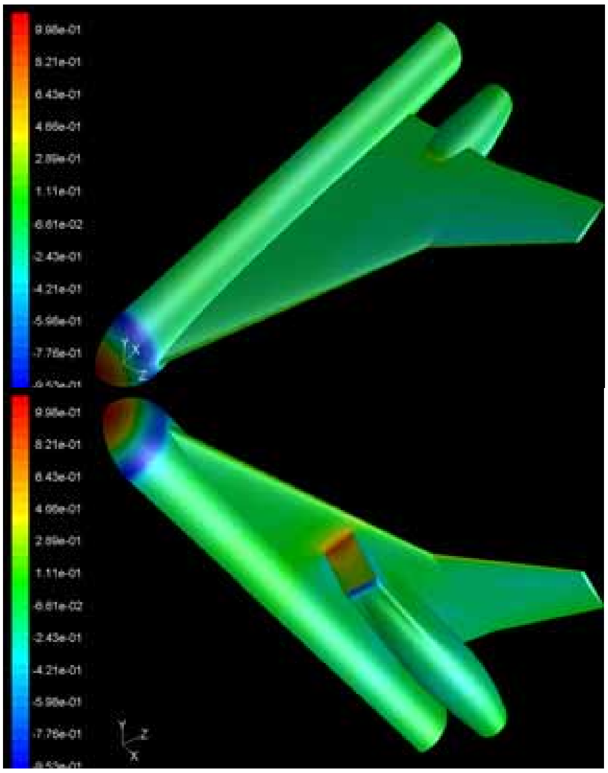

Fig. 15. Pressure Coefficient Contours M=.7, α =0.0

intake in a little larger area than the previous case. There are still no significant supersonic regions at this Mach number. Pressure contours and distributions for Mach number 0.9 are given in figures 20-22. Cp critical for this case is -0.1879. Supersonic regions appeared also on the outer board upper and lower wing surfaces. Most of the inboard are still subsonic.

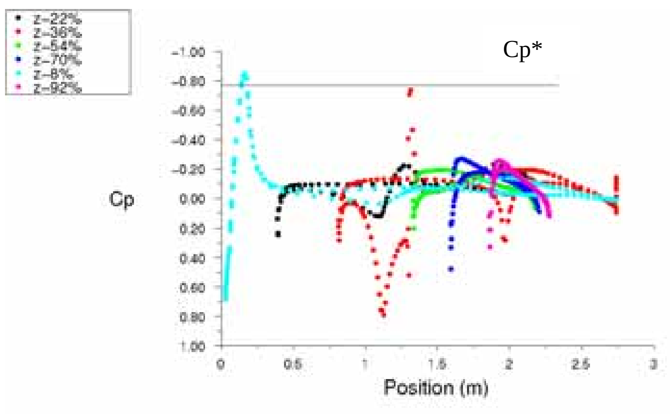

Fig. 16. Pressure Coefficient Distributions M=.7, α =0.0

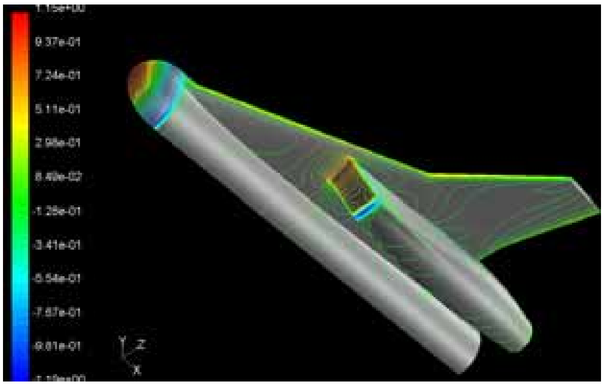
Fig. 17. Pressure Coefficient Contours *M*=.8, α =0.0

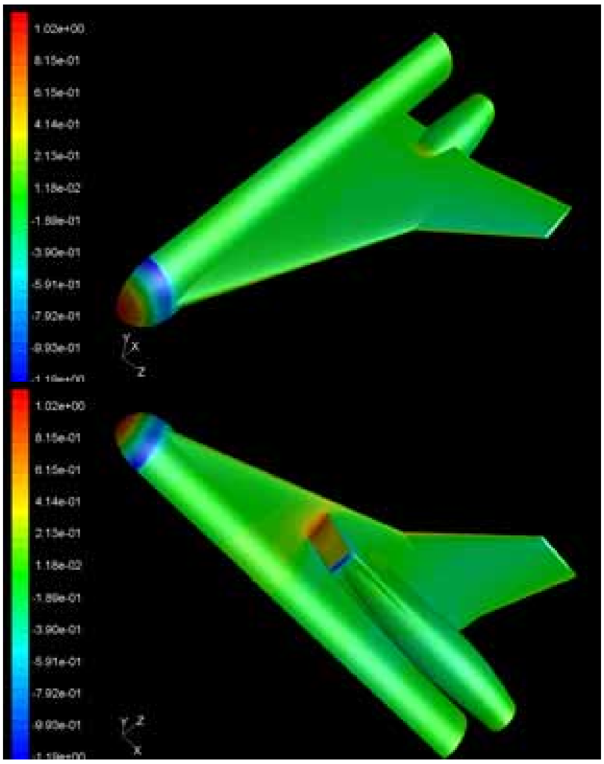
Fig. 18. Pressure Coefficient Contours *M*=.8, α =0.0

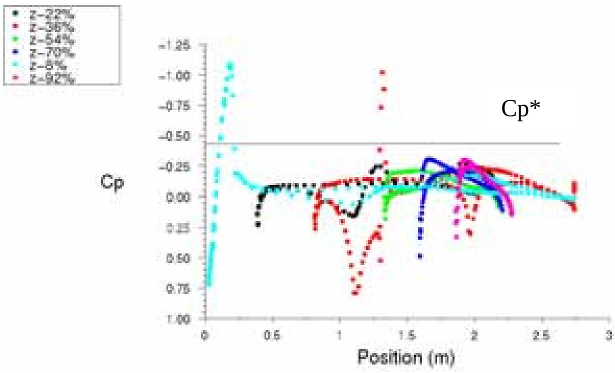

Fig. 19. Pressure Coefficient Distributions *M*=.8, α =0.0

A strong shock wave was established on the surface of engine, which propagated to the lower surface of the outer wing and to the fuselage, too. There are no shock waves on the upper wing surface in this case.

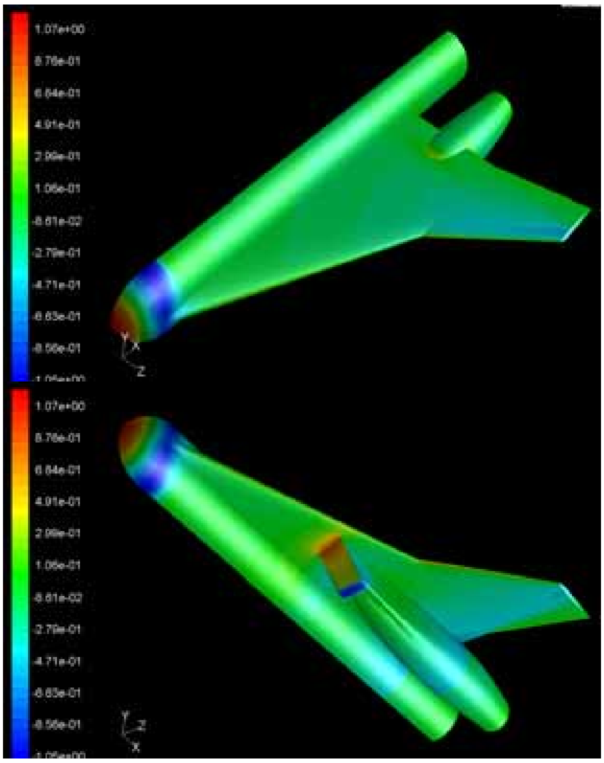
Fig. 20. Pressure Coefficient Contours *M*=.9, α =0.0

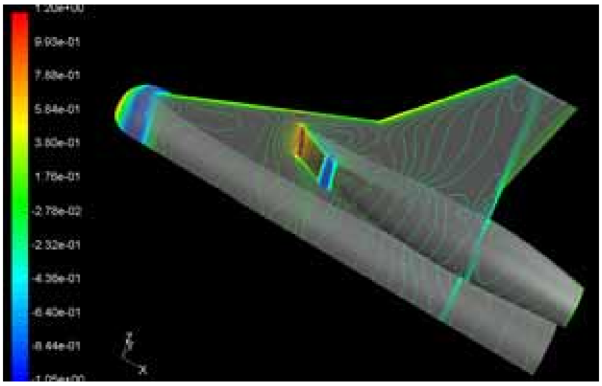
Fig. 21. Pressure Coefficient Contours *M*=.9, α =0.0

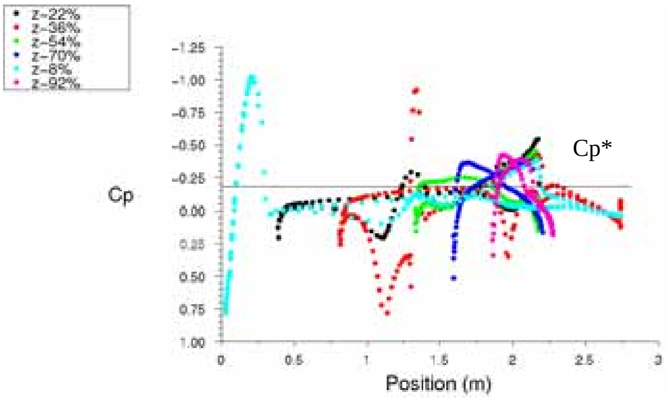

Fig. 22. Pressure Coefficient Distributions M=.9, α =0.0

3.2 CONCLUSIONS

(1) The single-block solver is used to investigate the flow around a SST type wing and its results were verified through an inter-code validation between JAXA and DLR. The effect of oscillation of control surface in transonic region (at the considered flow conditions, amplitude and frequencies) on a thin wing was investigated.

(2) A multi-block/overset grid solver is developed and verified through different test cases. The results showed considerably good agreement with other references or methods. This code can be run on parallel computers using MPI, too. At present, there are some limitations on configurations of overset grid and multi-block grid. Further investigation and improvement are needed for this new code to be more reliable and to get more generality.

(3) The newly developed code will be promising to be powerful tool for the various aeroelasticity analyses, especially to reveal mechanisms of the complicated transonic flutter of the wing with stores.

References

[1] Baldwin, B.S. and Lomax, H., Thin Layer Approximation and Algebraic Model for Separated Turbulent Flows, *AIAA Paper 78-257, 1978.*

[2] Yee, H. and Harten, A, Implicit TVD Schemes for Hyperbolic Conservation Law in Curvilinear Coordinates, *AIAA Paper 85-1513.*

[3] Kkeirandish, H., Goro, B. and Nakamichi, J., Numerical Investigation of Flutter, *International Journal of Computational Fluid Dynamics, 1999, Vol.12, pp. 279-290*

[4] Steger,J. and Dougherty, F. A Flexible Grid Embedding Technique with Application to the Euler Equations, *AIAI paper 83-1944*

[5] [5] Tamayama, M., Saitoh, K., Matsushita, H. and Nakamichi, J., Data Set: SST Arrow Wing, Oscillating Flap, *AGARD Unsteady Aerodynamics Working Group 22.*

[6] Wegner, W., Aerodynamics for Elastically Oscillating Wings Using the Virtual Grid Deformation Method, *report r-822, 85th AGARD/RTO Meeting, Aalborg, 1997*

[7] J. Nakamichi H.R Kheirandish, Nonlinear Flutter Simulation of NAL Non-powered SST Experimental Airplane and Related Wind Tunnel Tests, *CEAS/AIAA/AIAE International Forum on Aeroelasticity and Structural Dynamics 2001/04/10*,(Madrid

[8] Yee, H. , Linearized Form of Implicit TVD Schemes for The Multidimensional Euler and Navier-Stokes Equations, *journal of Comp& Maths with Appls. Vol 12A. Nos. 4/5. pp. 413-432, 1986.*

[9] Tannehill .J.C., Anderson D.A., Pletcher R.H., (1997). *Computational Fluid Mechanics and Heat Transfer,* Taylor & Francis.

[10] Kawasaki Heavy Industry KR-14465 (in Japanese) 4 Archiving